CHINESE OPTICS LETTERS

Vol. 23, No. 1 | January 2025

Real-time synchronous detection of wind and aerosol using a coherent lidar

Yue Shi (史 悦)[1,2], Xiong Luo (罗 雄)[1,3*], Peiyu Sun (孙培育)[2], Jihui Dong (董吉辉)[1,4**], Lei Tang (汤 磊)[5], Jie Zhou (周 杰)[1,3], Ke Wang (王 柯)[1,3], Chunli Chen (陈春利)[1,3], Yunshi Wang (王云石)[1,3], and Dingfu Zhou (周鼎富)[1,3,4***]

[1] Southwest Institute of Technical Physics, Chengdu 610041, China

[2] Science College, Civil Aviation Flight University of China, Guanghan 618307, China

[3] Lidar and Device Laboratory, Southwest Institute of Technical Physics, Chengdu 610041, China

[4] Key Laboratory of Laser Device Technology of China North Industries Group Corporation Limited, Chengdu 610041, China

[5] China Research and Development Academy of Machinery Equipment, Beijing 100089, China

*Corresponding author: luoxiong1987@163.com

**Corresponding author: j.h.dong@163.com

***Corresponding author: df_xh_zhou@sina.com

Received June 12, 2024 | Accepted July 29, 2024 | Posted Online February 18, 2025

Coherent lidar (CL) addresses existing constraints in CL data products by enabling simultaneous observation of multiple meteorological parameters such as cloud height, extinction coefficient, aerosol concentration, and wind field evaluation. A detailed analysis of CL echo signals was performed at a wavelength of 1550 nm, enabling accurate measurements of cloud height and aerosol concentration. Extensive data analyses and validation tests were conducted, aligning them with a 532 nm direct aerosol lidar (AL). The assessments of the aerosol extinction coefficient demonstrated notable consistency. This underscores the potential of advanced CL for providing prolonged and consistent observations across diverse meteorological conditions.

Keywords: coherent lidar; aerosol extinction coefficient; aerosol concentration; wind.

DOI: 10.3788/COL202523.011203

1. Introduction

Aerosols play a pivotal role in natural systems, impacting air pollution[1], cloud nucleation[2], precipitation distribution[3], and variations[4] by modulating solar radiation[5,6]. Thorough insights into aerosol transport dynamics can greatly advance the design and implementation of effective air pollution mitigation measures[7]. Thus, obtaining synchronized datasets on aerosols and wind is crucial. Rigorous observation and analysis of these factors are essential for tracking climate patterns and understanding their implications for both environmental and societal well-being[8,9].

Relative to traditional lidar, coherent lidar (CL) offers distinct benefits, including a more compact design, lower power consumption, and increased adaptability in detection modalities. As a result, coherent Doppler wind lidar technology has become the predominant technique for wind field detection[10–14] and has the ability to meet the requirements of high-precision measurements. Prolific research and subsequent advancements underscore the vital and efficacious role of CL in diverse fields, encompassing atmospheric studies, wind energy sectors, and aviation safety[15–19]. Nonetheless, it is imperative to recognize that most contemporary CL systems predominantly utilize Doppler frequency shift data derived from the echo signal spectrum to determine wind velocities[20–24], or integrate additional devices to capture meteorological parameters[25–27].

Several studies have demonstrated the correlation between CLs and aerosols or boundary layer height. Menzies and Tratt[28] (1994) utilized a CO_2 airborne CL (near 9 μm) to obtain the vertical distribution of backscatter in the troposphere and lower stratosphere after hard target calibration. Chouza *et al.*[29] (2015) employed a 2 μm airborne Doppler wind lidar and calibrated a ground-based 532 nm direct aerosol lidar (AL) using a sun photometer for comparison, with error results within 20% for the backscatter and extinction profiles. Abdelazim *et al.*[30] (2015) used a 1.5 μm all-fiber coherent Doppler lidar, with the carrier-to-noise ratio (CNR) as a distance-squared correction signal, to obtain aerosol backscatter coefficient and wind speed. Dong *et al.*[31] (2018) simulated the process of aerosol particle backscattering of a horizontally polarized laser using a semi-analytical Monte Carlo method, analyzing the characteristics of laser backscatter under various

meteorological conditions and providing reference for CL systems. Wang *et al.*[32] (2019) combined the direct detection lidar for PM2.5 with the coherent Doppler wind lidar, both at 1.5 μm, and used the CNR along with vertical wind speed to determine the boundary layer height. It indicates that CL can acquire relevant aerosol information through calibration with other instruments. However, further comparative analysis is still needed to obtain more information about measured variables beyond aerosols under various weather conditions.

Departing from traditional methodologies, this research aims to highlight the potential of compact CL technology for detecting a range of meteorological parameters, encompassing cloud height, aerosol extinction coefficient, and aerosol concentration, coupled with wind field evaluation. Especially, experimental comparisons of aerosols were conducted under multiple meteorological conditions. In light of this, the study introduces a comprehensive data-processing approach to extract these elements, leveraging a compact CL with a 1.55 μm operational wavelength.

2. System and Principles

Figure 1 illustrates the layout of our CL system. The 1550 nm seed laser with a linewidth of 10 kHz is split into two beams using a beam splitter. One beam enters the local oscillator, while the other is amplified by an erbium-doped fiber amplifier (EDFA), controlled to achieve a pulse energy of 150 μJ after passing through an acousto-optic modulator (AOM) and modulated by the control system with a radio frequency (RF) tone before being transmitted into the atmosphere. The atmospheric echo signal is received by a 100 mm telescope, part of a scanning system with an integrated transmitter and receiver controlled to avoid the blind zone. The aerosol scattering and local oscillator signals are then converted into a heterodyne electrical signal through coherent homodyne mixing, followed by signal processing.

The intermediate frequency current signals, emanating from the balanced detector, are generated by mixing echo signals with local oscillator signals,

$$I_{\mathrm{RF}} = 2\Re\sqrt{P_L P_S}\cos\left(2\pi\omega_d t + \Delta\varphi\right), \tag{1}$$

where P_L is the power of the local oscillator signal, P_S is the power of the echo signal, $\Re$ is the detector responsivity, ω_d is the beat frequency, and $\Delta\varphi$ is the phase difference between the local oscillator signal and the echo signal.

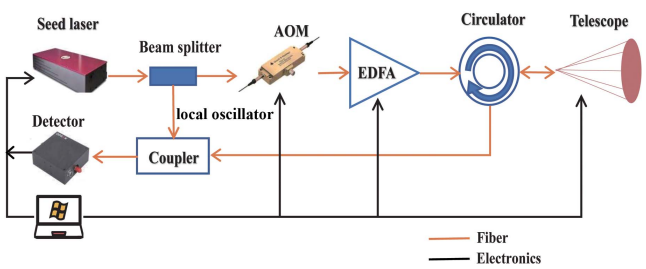

Fig. 1. The composition chart of the CL.

The current signal is converted to a voltage signal through impedance amplification in the detector. By applying a fast Fourier transform (FFT), it is possible to obtain the Doppler frequency shift of the aerosol, which can then be used to calculate the wind speed. Concurrently, the signal is processed to yield a sampling rate of S_R and a sample size of N from the detector, and this power is subsequently utilized for analyzing the spectral energy. The CL ultimately outputs a frequency-domain signal derived from time-frequency conversion. According to Parseval's theorem[33], the signal's energy remains constant during this conversion. Consequently, the power of the echo signal P_S is

$$P_S = \frac{S_R R_L}{2P_L\Re^2 G^2 \mathrm{N}} E_s = \frac{S_R R_L}{2P_L\Re^2 G^2 \mathrm{N}} E_f, \tag{2}$$

where R_L is the impedance of the signal acquisition and processing board, G is the amplification ratio of the balanced detector, Es is the energy of the acquired signal, and E_f is the signal energy from the spectral signal.

To accurately obtain the aforementioned parameters, it is crucial to make distance corrections to P_S:

$$S(r) = \ln\left(\frac{P_S}{I_z}\right), \tag{3}$$

where $S(r)$ is the correction of P_S and I_z is the correction factor related to the range r and the correction coefficient Δz, which is given by

$$I_z = \frac{\Delta z}{(r-\Delta z)^2 + \Delta z^2}, \tag{4}$$

where Δz depends on the focal length F, telescope radius a_t, and laser wavelength λ, as described by[34]

$$\begin{cases} \Delta z = \frac{F^2 z_r}{F^2 + z_r^2} \\ z_r = 2\pi\lambda\left(\frac{F}{a_t}\right)^2 \end{cases}. \tag{5}$$

The range corrected signal $S(r)$ is utilized for subsequent inversion calculations to determine the aerosol extinction coefficient, then the cloud height, visibility, and aerosol concentration are all converted by the extinction coefficient. The parameters of the CL are shown in Table 1.

Since the accuracy of estimation of the frequency shift depends on the echo signal and noise power, the signal-to-noise ratio (SNR)[35] is an important characteristic in terms of the possibility of sensing the atmosphere using a CL:

$$\mathrm{SNR} = \frac{\eta E c}{h\nu B} T^2(r)\beta(r)\frac{S_c(r)}{r^2}, \tag{6}$$

where η is the quantum efficiency of the detector, E is the pulse energy, c is the speed of light, h is the Plank's constant, υ is the

Table 1. System Parameters of the CL.

Symbol	Parameter	Value
$\Re$	Detector responsivity (A/W)	1
G	Electronics conversion gain (V/A)	30000
R_L	Impedance (Ω)	50
S_R	Signal sampling rate (MHz)	400
N	Number of sampling points	512
P_L	Power of the local oscillator signal (mW)	0.5
F	Focal length (m)	5000
a_t	Telescope radius (mm)	50
E	Pulse energy (μJ)	150
B	Receiving bandwidth (MHz)	200

laser's frequency, B is the detector's bandwidth, T is the atmospheric transmittance, β is the backscatter coefficient of aerosol particles, and $S_c(r)$ is the area of the coherent plate, which are related to the coherence radius of the backscattered wave in the telescope plane[36]. Consequently, the SNR is influenced by several parameters, including aerosol characteristics, coherence radius of the echo signal, detector quantum efficiency, and wavelength. Among them, the strength of refractive turbulence represents the atmospheric inhomogeneity, which compromises the spatial coherence of the scattered waves in the detection beam and the telescope plane, leading to the deterioration of the SNR. Under standard atmospheric conditions, the SNR at the distance of 1 km is approximately 11 to 26 dB (affected by turbulence intensity).

The operational principle and algorithmic procedure of the CL, applied to the detection of wind field, cloud height, visibility, and aerosol concentration, are illustrated in Fig. 2. Eight steps for extracting the mentioned key observable associated with winds and aerosols are as follows:

(a) In order to calculate the power of the signal P_S and the SNR, it is necessary to convert the signal from the time domain to the frequency domain. This includes performing a Fourier transform on the signal, which breaks it down into its frequency components. By analyzing the frequency domain information, it is possible to determine the frequency shift, total energy of the signal, and quality of the signal.
(b) The wind speed and direction are calculated using the zenith angle and azimuth angle of the lidar, which provides valuable information on the atmospheric flow field.
(c) The distance correction of P_S yields the signal $S(r)$, which is then calibrated using a linear regression equation through piecewise linear fitting.
(d) The maximum coefficient of correlation in the linear regression equation is then used to calculate the extinction coefficient σ_0 and position r_0 (reference distance) using the Collis slope method.
(e) The extinction coefficient is calculated using the Klett method[37], which involves performing backward integration for $r - r_0$ and forward integration for $r_0 - r$, providing an accurate estimate of the extinction coefficient.
(f) For cloud height measurement, a comprehensive approach is employed, involving the threshold method, differentiation method, and aerosol extinction coefficient method to determine the cloud base height from the echo signal.
(g) Visibility measurement involves converting the extinction coefficient to visibility and using the wavelength corrected q for the corresponding wavelength[38].
(h) Finally, aerosol concentration measurement is achieved using an exponential model[39], where calibration parameters, a, b, and c, are obtained by measuring multiple sets of aerosol concentration values using standard equipment at the same location.

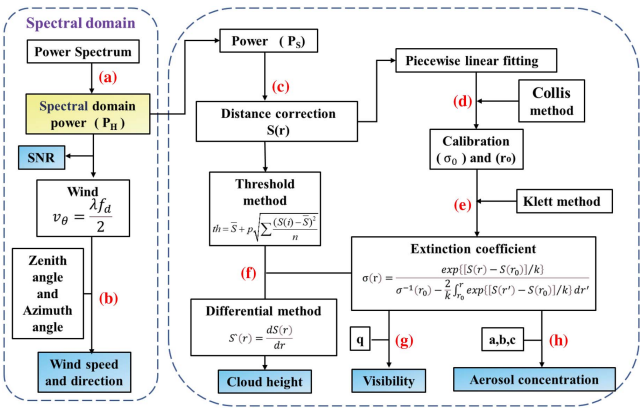

Fig. 2. Data processing procedure of wind, cloud height, extinction coefficient, visibility, and aerosol concentration.

3. Experiment and Results

Between March and April 2022, a side-by-side experiment was executed in Chengdu, China. The study employed CL with an operational wavelength of 1550 nm and a dual-polarization aerosol detection lidar set to a 532 nm wavelength. The evaluation spanned multiple meteorological scenarios, encompassing sunny, cloudy, rainy, and foggy conditions. The experimental setup is illustrated in Fig. 3.

The systems of the two different devices were compared in Table 2, revealing significant differences between the two lidar types. The CL is different from the AL in the principle of heterodyne coherent detection. The CL, using a 1550 nm wavelength, is capable of measuring the wind field while also capturing extinction coefficients, cloud height, and visibility. On the other hand, the AL is a direct detection lidar based on the Mie scattering principle, using a 532 nm wavelength to measure aerosol related

Fig. 3. Experimental scene.

parameters. It can measure extinction coefficients, visibility, PM10 and PM2.5 aerosol concentrations, and depolarization ratio.

Compared to the AL, the CL presents superior applicative advantages, including enhanced detection efficiency, a streamlined structure, and a more comprehensive range of data products. This technology can concurrently measure cloud height, extinction coefficient, visibility, aerosol concentration, and wind field. Employing a singular apparatus diminishes the intricacy of the detection system, bolsters system stability, and augments adaptability for mobile detection tasks, specifically in domains such as meteorological support and environmental pollution monitoring.

The aerosol concentration was measured under various meteorological conditions, including sunny, cloudy, rainy, and foggy days. An analysis of aerosol extinction coefficients under these distinct weather conditions is presented in Figs. 4 and 5, and is compared in Table 3.

Heavy haze resulted in reduced visibility, with the measurements from both instruments closely aligned, as demonstrated in Figs. 4 and 5(a), which present a comparison of detected aerosol extinction coefficient and SNR. During daytime, the haze induced reduced visibility and SNR, with the cloud layer observed at a relatively low altitude.

On gloomy and rainy days, the aerosol extinction coefficient and SNR detected by both instruments aligned with the atmospheric conditions, as depicted in Figs. 4 and 5(b). Both devices registered analogous trends in their measurements, with the identification of cloud layers aligning consistently. Throughout the day, from dawn to dusk, the atmospheric structure in the

Table 2. Comparison of the CL and AL.

System	CL	AL
Wavelength (nm)	1550	532
Detection mode	Coherent detection	Direct detection
Range (km)	10	15
Antenna	T-R combine, 100 mm	T-R separate, 160 mm
Pulse energy (μJ)	150	20
Pulse repetition rate (kHz)	10	2
Range resolution (m)	15–200 (adjustable)	15
Wind speed accuracy (m/s)	0.5	—
Wind direction accuracy (deg)	3	—
Azimuth scanning range (deg)	0–360	—
Zenith scanning range (deg)	0–90	90
Weight (kg)	60	—
Data product	Wind; extinction coefficient; aerosol concentration; visibility; cloud height	Extinction coefficient; visibility; PM10; PM2.5; depolarization ratio
Advantage	Without geometric factor; eye-safe; high sensitivity; high time resolution	Visible light; closer to human visibility
Disadvantage	Secondary data acquisition time; invisible light; data conversion required	Long acquisition time; not eye-safe; blind zone; geometric factor correction required

Table 3. Comparison of the Aerosol Concentration and SNR.

Item	Weather	Figure	Aerosol concentration
2022/3/24	Hazy day	(a)	Closely aligned
2022/3/30	Overcast and rainy day	(b)	Congruent; during precipitation events (21:00-0:00), data from CL were missing, while AL continued, although its reliability is not high due to the rain
2022/4/5	Foggy day	(c)	Propinquity; the data gaps between 0:00 to 9:00 in AL may be caused by geometric factors

lower troposphere remained relatively unchanged, maintaining consistent aerosol concentrations and SNRs. However, during precipitation events, data from the CL were absent due to rain-induced interference. In contrast, the AL continued to yield data, although its accuracy was compromised by significant errors stemming from the rainfall, thus reducing its reliability.

The extremely low visibility weather conditions such as heavy fog significantly constrained the detection range of two lidar systems tasked with monitoring the aerosol extinction coefficient and SNR, as delineated in Figs. 4 and 5(c). Under conditions of dense fog characterized by remarkably low visibility, the detection range for both systems was curtailed, often restricted to less than 1 km. The data gap in the AL between 0:00 and 9:00 could be attributed to geometric factors. Moreover, the SNR value for the AL at altitudes below 6 km is notably high. The inconsistency in SNR could stem from unreliable AL measurements. Geometric constraints and high aerosol concentrations might cause AL saturation, leading to data loss and yielding incorrect SNR data.

Under most weather conditions, the results of the aerosol extinction coefficient and SNR by the two lidars are generally consistent. However, during certain weather conditions such as a rainy day and heavy fog, some factors such as laser wavelengths, polarization characteristics, and geometric factors can lead to varying results in the data products of the CL and AL.

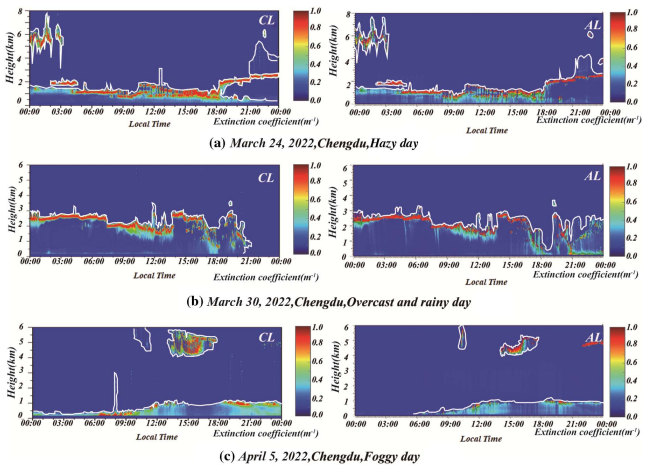

Fig. 4. Aerosol extinction coefficients in (a) a hazy day, (b) an overcast and rainy day, and (c) a foggy day.

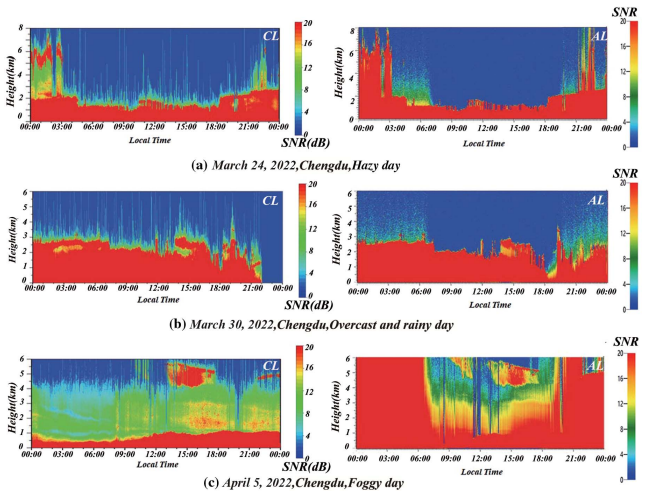

Fig. 5. SNRs in (a) a hazy day, (b) an overcast and rainy day, and (c) a foggy day.

4. Extinction Coefficient, Cloud Height, and Wind Field

In October 2022, a series of experiments were conducted based on the CL in Chengdu to collect comprehensive data products. The experiment yielded results for extinction coefficients, cloud height, wind field, and SNR data over a continuous period of 48 h, as illustrated in Fig. 6.

Figure 6(a) demonstrates a strong correlation among the aerosol extinction coefficient, cloud height, and wind field with the SNR depicted in Fig. 6(b). This correlation implies the accuracy and reliability of the measurements. On November 11, 2022, from noon to evening, a significant presence of aerosols was detected in the atmosphere, predominantly concentrated around a height of 1.5 km. These high concentrations of aerosols facilitated the formation of cloud clusters, as indicated by elevated extinction coefficient values. During this period, the wind remained relatively calm, with speeds ranging from 1 to 2 m/s. In the evening, at an altitude of 2 km, wind speeds increased to 6–8 m/s, concurrent with cloud formation at the same altitude. These stronger winds caused the clouds to move more rapidly, resulting in a shorter duration of the high aerosol concentration area. From the 12th, low visibility and wind speeds of approximately 1–2 m/s contributed to the accumulation of aerosols, leading to high aerosol levels at a distance of

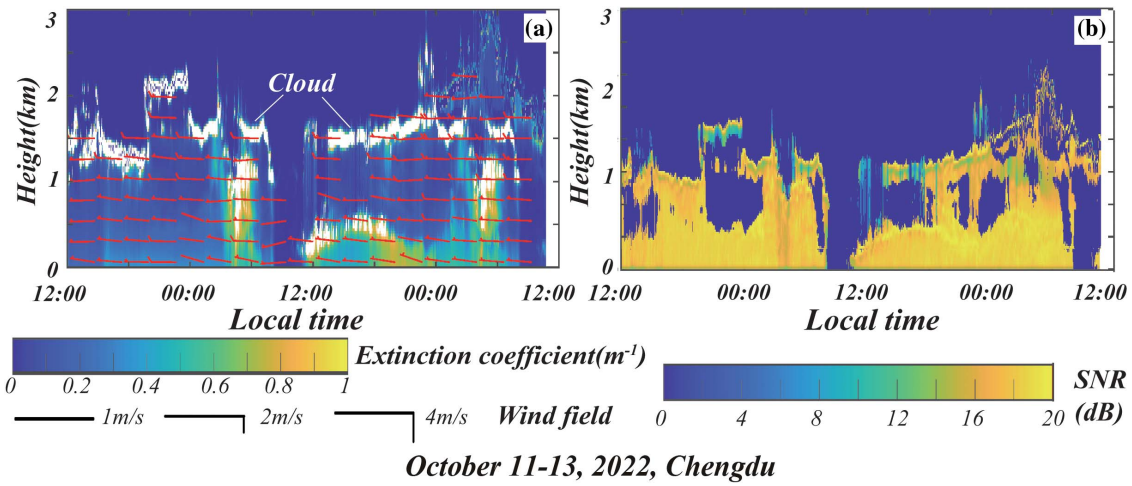

Fig. 6. October 11-13, 2022, Chengdu. (a) Data fusion of extinction coefficient, cloud height, and wind field. (b) SNR.

1 km. In the afternoon, there was a low SNR due to the rain, and then cloud clusters formed at altitudes of 1.5 km and 500 m, persisting until midnight. From 00:00 on the 13th, the wind speed escalated to 8 m/s, while clusters of clouds emerged at an altitude of 1.5 km.

Simultaneous measurement of meteorological factors such as wind, aerosols, and clouds enables more precise atmospheric monitoring. This approach provides accurate insights into the formation and dissipation of aerosol clouds and supports meteorological disaster warnings. Additionally, it serves as a basis for environmental preservation and pollution control measures.

5. Conclusion

In this investigation, the newly developed CL facilitates the determination of diverse meteorological parameters, including cloud height, extinction coefficient, visibility, and aerosol concentration, while concurrently assessing the wind field. This study examines the characteristics of the CL signal echoes, establishing a technique for calculating the echo signal power in the time domain. The Klett algorithm is employed to determine the atmospheric extinction coefficient, after which methods involving differential thresholds and aerosol extinction coefficients are used to derive cloud heights. Additionally, atmospheric visibility and aerosol concentration are inferred based on their relationship with the extinction coefficient.

The developed CL consistently demonstrates its capability to measure a range of meteorological parameters, such as horizontal wind speed and direction, cloud height, visibility, extinction coefficient, and aerosol concentration under diverse weather conditions including sunny, cloudy, rainy, and foggy scenarios. Integrating this CL for comprehensive meteorological observations offers benefits in terms of simplicity, compactness, and system robustness while also enhancing mobile detection capabilities. The amalgamation of these meteorological parameters results in a rich set of secondary data products, notably aerosol flux products. Beyond merely tracking pollutant locations and concentrations, the CL provides tools for pinpointing pollutant origins, gauging dispersion velocities and trajectories, and forecasting pollutant movement patterns, thereby aiding in the implementation of effective interventions.

Acknowledgements

This work was supported by the Sichuan Science and Technology Plan Project (No. 2022YFG0352).

References

1. R. Volkamer, J. L. Jimenez, F. San Martini, *et al.*, "Secondary organic aerosol formation from anthropogenic air pollution: rapid and higher than expected," Geophys. Res. Lett. **33**, L17811 (2006).
2. J. H. Seinfeld, C. Bretherton, K. S. Carslaw, *et al.*, "Improving our fundamental understanding of the role of aerosol-cloud interactions in the climate system," Proc. Natl. Acad. Sci. U.S.A. **113**, 5781 (2016).
3. M. Andreae and D. Rosenfeld, "Aerosol–cloud–precipitation interactions. Part 1. The nature and sources of cloud-active aerosols," Earth Sci. Rev. **89**, 13 (2008).
4. Z. Li, W.-M. Lau, V. Ramanathan, *et al.*, "Aerosol and monsoon climate interactions over Asia," Rev. Geophys. **54**, 866 (2016).
5. U. Lohmann and J. Feichter, "Global indirect aerosol effects: a review," Atmos. Chem. Phys. **5**, 715 (2005).
6. H. Yu, Y. Kaufman, M. Chin, *et al.*, "A review of measurement-based assessments of the aerosol direct radiative effect and forcing," Atmos. Chem. Phys. **6**, 613 (2006).
7. Y. Yang, L. M. Russell, S. Lou, *et al.*, "Dust-wind interactions can intensify aerosol pollution over eastern China," Nat. Commun. **8**, 15333 (2017).
8. D. W. Griffin, C. A. Kellogg, and E. A. Shinn, "Dust in the wind: long range transport of dust in the atmosphere and its implications for global public and ecosystem health," Global Change Human Health **2**, 20 (2001).
9. E. L. Anderson, P. Turnham, J. R. Griffin, *et al.*, "Consideration of the aerosol transmission for COVID-19 and public health," Risk Anal. **40**, 902 (2020).
10. R. Menzies and R. Hardesty, "Coherent doppler lidar for measurements of wind fields," Proc. IEEE **77**, 449 (1989).
11. M. J. Kavaya, J. Y. Beyon, G. J. Koch, *et al.*, "The Doppler aerosol wind (dawn) air borne, wind-profiling coherent-detection lidar system: overview and preliminary flight results," J. Atmos. Ocean. Technol. **31**, 826 (2014).
12. Z.-H. Yang, Y.-K. Zhang, J. Zhou, *et al.*, "Real-time wind field measurements using all-fiber mobile Doppler wind lidar," Opt. Eng. **59**, 034107 (2020).

13. O. Kliebisch, H. Uittenbosch, J. Thurn, *et al.*, "Coherent doppler wind lidar with real-time wind processing and low signal-to-noise ratio reconstruction based on a convolutional neural network," Opt. Express **30**, 5540 (2022).
14. C. Liang, C. Wang, X. Xue, *et al.*, "Meter-scale and sub-second-resolution coherent doppler wind lidar and hyperfine wind observation," Opt. Lett. **47**, 3179 (2022).
15. J. Chu, Y. Han, D. Sun, *et al.*, "Statistical interpolation technique based on coherent Doppler lidar for real-time horizontal wind shear observations and forewarning," Opt. Eng. **60**, 046102 (2021).
16. G. J. Koch, J. Y. Beyon, L. J. Cowen, *et al.*, "Three-dimensional wind profiling of offshore wind energy areas with airborne Doppler lidar," J. Appl. Remote Sens. **8**, 083662 (2014).
17. R. Krishnamurthy, A. Choukulkar, R. Calhoun, *et al.*, "Coherent doppler lidar for wind farm characterization," Wind Energy **16**, 189 (2013).
18. S. Wu, J. Yin, B. Liu, *et al.*, "Characterization of turbulent wake of wind turbine by coherent Doppler lidar," Proc. SPIE **9262**, 92620H (2014).
19. Z. Liu, L. Yuan, J. Tang, *et al.*, "Coherent Doppler lidar wind retrieval for a typhoon based on the genetic simulated annealing algorithm," Chin. Opt. Lett. **22**, 040101 (2024).
20. R. Frehlich, "Coherent Doppler lidar signal covariance including wind shear and wind turbulence," Appl. Opt. **33**, 6472 (1994).
21. S. M. Hannon, J. A. L. Thomson, S. W. Henderson, *et al.*, "Windshear, turbulence, and wake vortex characterization using pulsed solid state coherent lidar," Proc. SPIE **2464**, 94 (1995).
22. M. Sjöholm, T. Mikkelsen, J. Mann, *et al.*, "Spatial averaging-effects on turbulence measured by a continuous-wave coherent lidar," Meteorol. Z. **18**, 281 (2009).
23. J. Yuan, H. Xia, T. Wei, *et al.*, "Identifying cloud, precipitation, windshear, and turbulence by deep analysis of the power spectrum of coherent doppler wind lidar," Opt. Express **28**, 37406 (2020).
24. P. Jiang, J. Yuan, K. Wu, *et al.*, "Turbulence detection in the atmospheric boundary layer using coherent Doppler wind lidar and microwave radiometer," Remote Sens. **14**, 2951 (2022).
25. S. Chen, J. Yu, M. Petros, *et al.*, "Double-pass Tm:Ho:YLF amplifier at 2.05 μm for spaceborne eye-safe coherent Doppler wind lidar and CO_2 differential absorption lidar (DIAL)," Proc. SPIE **4893**, 217 (2003).
26. F. Gibert, D. Edouart, C. Cénac, *et al.*, "2-μm Ho emitter-based coherent DIAL for CO_2 pro- filing in the atmosphere," Opt. Lett. **40**, 3093 (2015).
27. N. Cezard, S. L. Mehaute, J. Le Gouët, *et al.*, "Performance assessment of a coherent dial doppler fiber lidar at 1645 nm for remote sensing of methane and wind," Opt. Express **28**, 22345 (2020).
28. R. T. Menzies and D. M. Tratt, "Airborne CO_2 coherent lidar for measurements of atmospheric aerosol and cloud backscatter," Appl. Opt. **33**, 5698 (1994).
29. F. Chouza, O. Reitebuch, S. Groß, *et al.*, "Retrieval of aerosol backscatter and extinction from airborne coherent Doppler wind lidar measurements," Atmos. Meas. Tech. **8**, 2909 (2015).
30. S. Abdelazim, D. Santoro, M. F. Arend, *et al.*, "Development and operational analysis of an all-fiber coherent doppler lidar system for wind sensing and aerosol profiling," IEEE Trans. Geosci. Remote Sens. **53**, 6495 (2015).
31. X. Dong, Y. Hu, S. Xu, *et al.*, "Echoing characteristics of coherent lidar in different aerosol environments," Acta Opt. Sin. **38**, 0101001 (2018).
32. C. Wang, M. Jia, H. Xia, *et al.*, "Relationship analysis of PM2.5 and boundary layer height using an aerosol and turbulence detection lidar," Atmos. Meas. Tech. **12**, 3303 (2019).
33. H. K. Hughes, "The physical meaning of Parseval's theorem," Am. J. Phys. **33**, 99 (1965).
34. V. A. Banakh, I. N. Smalikho, and C. Werner, "Effect of aerosol particle microstructure on cw Doppler lidar signal statistics," Appl. Opt. **39**, 5393 (2000).
35. V. A. Banakh and I. N. Smalikho, *Coherent Doppler Wind Lidars in a Turbulent Atmosphere* (Artech House, 2013).
36. R. G. Frehlich and M. J. Kavaya, "Coherent laser radar performance for general atmospheric refractive turbulence," Appl. Opt. **30**, 5325 (1991).
37. J. D. Klett, "Lidar inversion with variable backscatter/extinction ratios," Appl. Opt. **24**, 1638 (1985).
38. G. J. McCartney, *Optics of Atmoshpere* (John Wiley & Sons, 1976).
39. D. Han, W. Liu, J. Liu, *et al.*, "Retrieval method for aerosol mass concentration vertical distribution," Chin. J. Lasers **33**, 1567 (2006).